JOURNAL OF VIROLOGY, July 2006, p. 6575–6587 Vol. 80, No. 13
0022-538X/06/$08.00+0 doi:10.1128/JVI.00347-06

Simian Virus 40 Late Proteins Possess Lytic Properties That Render Them Capable of Permeabilizing Cellular Membranes

Robert Daniels,[1] Nasser M. Rusan,[2]† Anne-Kathrin Wilbuer,[1]‡ Leonard C. Norkin,[3] Patricia Wadsworth,[2] and Daniel N. Hebert[1]*

Departments of Biochemistry and Molecular Biology,[1] Biology,[2] and Microbiology,[3] Program in Molecular and Cellular Biology, University of Massachusetts, Amherst, Massachusetts 01003

Received 17 February 2006/Accepted 18 April 2006

Many nonenveloped viruses have evolved an infectious cycle that culminates in the lysis or permeabilization of the host to enable viral release. How these viruses initiate the lytic event is largely unknown. Here, we demonstrated that the simian virus 40 progeny accumulated at the nuclear envelope prior to the permeabilization of the nuclear, endoplasmic reticulum, and plasma membranes at a time which corresponded with the release of the progeny. The permeabilization of these cellular membranes temporally correlated with late protein expression and was not observed upon the inhibition of their synthesis. To address whether one or more of the late proteins possessed an inherent capacity to induce membrane permeabilization, we examined the permeability of *Escherichia coli* that separately expressed the late proteins. VP2 and VP3, but not VP1, caused the permeabilization of bacterial membranes. Additionally, VP3 expression resulted in bacterial cell lysis. These findings demonstrate that VP3 possesses an inherent lytic property that is independent of eukaryotic signaling or cell death pathways.

To establish a viral infection within a host, it is essential that the viral genome is delivered in a replication-competent form and the progeny are released in an infectious state. Although simple in nature, these requirements are hindered by the complex network of macromolecule-impermeable membranes that are present within eukaryotic cells. To circumvent these problems, viruses have evolved strategies to traverse or penetrate cellular membrane barriers during the infection and release processes (reviewed in references 15, 30, and 36). Once infected, the host cellular machinery is redirected by the virus to facilitate the replication of its own genome and the synthesis of the viral enzymes and structural components that are necessary to assemble the progeny virions. Following replication, the cellular integrity that hinders the dissemination of the nonenveloped virions becomes dispensable.

Nonenveloped DNA viruses are assembled in the nucleus. Therefore, the viral progeny must pass through the contiguous nuclear/endoplasmic reticulum membranes and the plasma membrane without becoming enveloped during the release process. Nonenveloped DNA viruses are believed to avoid these problems by inducing necrosis (10, 12, 13). Necrosis is characterized by cellular swelling, rough endoplasmic reticulum (ER) fragmentation, and plasma membrane permeabilization that results in the extracellular release of cytosolic constituents and, ultimately, cell lysis (33, 34). While this is thought to be fundamental for this class of viruses, little is known about which cellular membranes are permeabilized and what the viral requirements are for this process that enables the release of the nonenveloped progeny.

As in the case of other DNA viruses, simian virus 40 (SV40) gene expression is temporally regulated such that viral genome replication occurs prior to the synthesis of the structural proteins. The SV40 early protein large T antigen is largely responsible for facilitating the replication of the viral genome and directing the synthesis of the capsid proteins VP1, VP2, and VP3 (3, 11, 16, 26, 29, 32). Upon synthesis, VP1 readily forms pentamers that contain a single copy of either VP2 or VP3 within their central cavity (1, 9). These VP1 pentamer-VP2/3 complexes are then imported into the nucleus, where 72 pentameric complexes assemble around the viral genome to create the icosahedral capsid (19).

This study shows that the SV40 progeny alter their nuclear localization prior to the detection of permeability changes in the nuclear, ER, and plasma membranes. The observed permeability changes occurred after late gene expression and were prevented by the selective inhibition of late gene expression, implying that one or more of these viral gene products were required for permeabilization of host membrane barriers. This hypothesis was tested by examining the permeabilization of *Escherichia coli* upon the expression of the late proteins. We found that VP2 and VP3 were capable of permeabilizing bacterial membranes. Furthermore, VP3-induced permeabilization resulted in bacterial cell lysis, demonstrating that VP3 possesses an intrinsic lytic property.

* Corresponding author. Mailing address: Department of Biochemistry and Molecular Biology, University of Massachusetts, Amherst, MA 01003. Phone: (413) 545-0079. Fax: (413) 545-3291. E-mail: dhebert@biochem.umass.edu.

† Present address: Biology Department, University of North Carolina, Chapel Hill, NC 27599.

‡ Present address: Department of Cancer Immunology and AIDS, Program in Immunology, Harvard Medical School, Boston, MA 02115.

MATERIALS AND METHODS

Reagents. African green monkey kidney cells (BS-C-1) were obtained from ATCC. Dulbecco's modified Eagle medium (DMEM), penicillin-streptomycin, fetal bovine serum, and HRP-linked antimouse and antirabbit antibodies were purchased from Invitrogen Inc. (Carlsbad, CA). VP1 and VP2/3 polyclonal antibodies were a generous gift from A. Oppenheim (Jerusalem, Israel). Large T antigen (LT) monoclonal antibody Ab-2 and the C-terminal and N-terminal calnexin antibodies were from Oncogene (San Diego, CA) and Stressgen (Vic-

toria, BC), respectively. The metalloendoprotease inhibitor benzyloxycarbonyl-Gly-Phe-NH_2 (zGF-NH_2) was from Bachem (Torrance, CA), and the proteasomal inhibitors LCT and ALLN were from Calbiochem (La Jolla, CA). All other reagents were from Sigma (St. Louis, MO).

Tissue culture and infections. BS-C-1 cells were maintained in DMEM-5% fetal bovine serum (FBS) with Pen-Strep in a humidified 5% CO_2 incubator at 37°C. SV40 viral lysates were obtained by infecting confluent BS-C-1 cells with ~0.05 multiplicity of infection (MOI) SV40. After 2 days, the medium was changed and replaced with DMEM-2% FBS with Pen-Strep. Cells were infected until all of the cells were dead ~12 days later. Cells were freeze-thawed three times. Cell debris was pelleted at 3,000 × *g* for 10 min at 27°C. The supernatant containing the virus was isolated and stored at −80°C. All infections were performed on dishes or glass coverslips containing confluent BS-C-1 cell monolayers. The MOI was ~0.5 and the infections were synchronized by prebinding the virus at 4°C for 2 h while rocking. The residual unbound virus was removed and replaced with fresh DMEM, 2% FBS, and Pen-Strep before shifting cells to 37°C to initiate endocytic uptake.

Immunoblotting and trypan blue analysis. Cell lysates were prepared from the total cell population combining nonadherent and adherent cells. At each time point, the medium was retained, the nonadherent cells were sedimented at 8,000 × *g* for 5 min at 4°C, the medium was transferred to a new tube, and the cellular debris was retained. The adherent cells were washed twice with phosphate-buffered saline (PBS) and lysed on ice in the dish using lysis buffer (1% NP-40–HEPES-buffered saline (50 mM HEPES, 200 mM NaCl [pH 7.5]), 2.4 mM *N*-ethylmaleimide, 50 μM *N*-Leu-Leu-norleucinol, 0.4 μM phenylmethylsulfonyl fluoride, and 20 μM leupeptin) and collected by scraping. The cell lysate from the dish was combined with the sedimented, nonadherent cells, and the protein concentration was determined by Bradford analysis. For each experiment, the indicated protein concentration of the total cell lysate, or overlay media, was resolved by sodium dodecyl sulfate-polyacrylamide gel electrophoresis (SDS-PAGE), and then the lysate was transferred to polyvinylidene difluoride membrane and immunoblotted. For trypan blue analysis, the cells were treated similarly, except the adherent cells were detached using trypsin-EDTA. The trypsinized and nonadherent cells were pooled, sedimented at 8,000 × *g* for 5 min at 4°C, washed twice in ice-cold PBS, and resuspended in PBS. The cells were mixed in a 1:1 ratio with trypan blue and the percentage of trypan blue-positive cells was determined from total cell populations by staining under a light microscope.

Immunocytochemistry. Glass coverslips containing cells were fixed with ice-cold 100% methanol at 4°C for 10 min. Methanol was removed and the coverslips were washed twice in PBS and rehydrated in PBS-0.1% Tween-0.2 gm/liter Azide (PBS-Tw-Az) at 4°C for 1 h. Cells were stained with a primary antibody to large T antigen or VP1 in 1% bovine serum albumin–PBS-Tw-Az for 1 h at 37°C at a dilution of 1:100. The coverslips were washed with PBS-Tw-Az and incubated with the appropriate secondary antibody according to the manufacturer's instructions. Coverslips were washed in PBS-Tw-Az and mounted on slides using Vectashield.

Microscopy and image analysis. Images were acquired with an inverted microscope (Eclipse TE3000; Nikon) equipped with a 10× phase objective, a spinning-disk confocal-scan head (PerkinElmer), and a MicroMax Interline Transfer cooled charge-coupled-device camera (Roper Scientific). Phase and corresponding fluorescent images were collected for each time point. MetaMorph was used for both image acquisition and analysis. The Region Tools function in MetaMorph was used to measure nuclear diameters.

For three-dimensional reconstruction experiments, fixed cells were imaged with a 100× (numerical aperture, 1.4) phase objective lens mounted on a p-721 piezo nanofocusing device (Physik Instruments, Auburn, MA). The entire volume between 1 μm above and 1 μm below the nucleus was imaged in 200-nm steps and subjected to blind, iterative deconvolution (Autoquant Imaging, Albany, NY). The AutoVisualize function in Autoquant was used to produce the image rotation.

Bacterial expression plasmids, *E. coli* membrane permeability, and viability. The entire coding sequences for VP1, VP2, and VP3 were amplified by PCR using primers that placed 5′ NheI and 3′ BamHI cleavage sites and cloned into the pET21d expression vector (Novagen, Madison, WI). GST-VP3 and -VP2 expression vectors were created similarly, using primers that placed 5′ BamHI and 3′ XhoI cleavage sites followed by cloning into the bacterial expression plasmid pGEX-6p1 (Amersham Bioscience, Piscataway, NJ). The vectors were verified by sequencing (Davis, CA) and transformed into the *E. coli* Rosetta strain (DE3: pLysS) for protein expression (Novagen). For permeability assays, cultures were grown in the presence of 75 μg/ml ampicillin at 37°C to an optical density (OD) at 600 nm of ~1.0, and protein expression was induced with 1 mM isopropyl-β-D-thiogalactopyranoside (IPTG) with 150 μg/ml rifampin for the indicated time followed by a 10-min pulse with 0.3 μCi [^{35}S]Met-Cys in the absence or presence of 500 μM hygromycin B (8). Bacterial cell lysis was monitored by following the OD at 600 nm after protein expression in cultures at an OD at 600 nm of ~0.20 was induced by the addition of 1 mM IPTG (37).

RESULTS

The death of SV40-infected cells follows the expression of the late genes. To establish a timeline for the completion of the SV40 lytic cycle, infected cells were stained for trypan blue, which indicates plasma membrane permeabilization and cell death. Trypan blue staining of SV40-infected cultures revealed that permeabilization of the plasma membrane and cell death first occurred at 60 h and increased over time (Fig. 1B). Thus, a full infection cycle under our conditions can be completed within 60 h, but the majority of the primary infections required 72 to 96 h.

To correlate the completion of the lytic cycle with the pattern of viral protein synthesis, we examined the temporal expression of the early and late genes in African green monkey kidney (BS-C-1) cells. While it is well established that SV40 expresses early and late genes, significant disparities exist throughout the literature with regard to the timing of their expression. The initiation of LT synthesis has been shown to occur from 8 to 24 h postinfection, that of VP1 from 3 to 24 h, and those of VP2 and VP3 from 33 to 48 h (3, 20, 21, 27, 38). Immunoblot analysis of lysates generated from BS-C-1 cells infected with ~0.5 MOI of SV40 showed that LT expression was induced by 12 h, while VP1, VP2, and VP3 expression initiated by 36 h (Fig. 1A and B). Thus, the death of the infected cell occurred ~48 h after the initiation of early gene expression and ~24 h after the initiation of late gene expression.

SV40 release follows the permeabilization of the nuclear and plasma membranes. Newly assembled SV40 virions must pass through the macromolecule-impermeable nuclear envelope and plasma membrane to exit the host cell. Therefore, we examined the integrity of the nuclear envelope by fixed cell confocal microscopy using LT as a marker for infection. In agreement with the protein expression profiles (Fig. 1A), LT was first observed at 12 h by immunofluorescence (Fig. 2A and C). While early gene expression initiated within 12 h, the large increase in the number of LT-positive cells from 12 to 48 h demonstrated that early gene expression in the majority of the cells occurred much later. During the initiation of early gene expression from 12 to 48 h, LT was strictly confined to the nucleus. However, a small portion of infected cells with a nonviable morphology showed diffuse LT staining throughout the cytoplasm by 60 h (Fig. 2A, compare a and a' to b). These findings indicate that the nuclear envelope was disrupted in a time-dependent manner, since the number of cells with diffuse cytoplasmic LT staining significantly increased from 60 to 96 h (Fig. 2C), when LT synthesis had ceased (Fig. 1, compare 72 to 96 h).

The appearance of cytoplasmic LT staining coincided with the increase in trypan blue staining, indicating that the nuclear membrane was likely disrupted in dead cells with a permeabilized plasma membrane (Fig. 1B, 2A, and C). While disruption of the nuclear membrane would account for the diffusion of LT into the cytoplasm, the additional permeabilization of the plasma membrane would result in the subsequent leaching

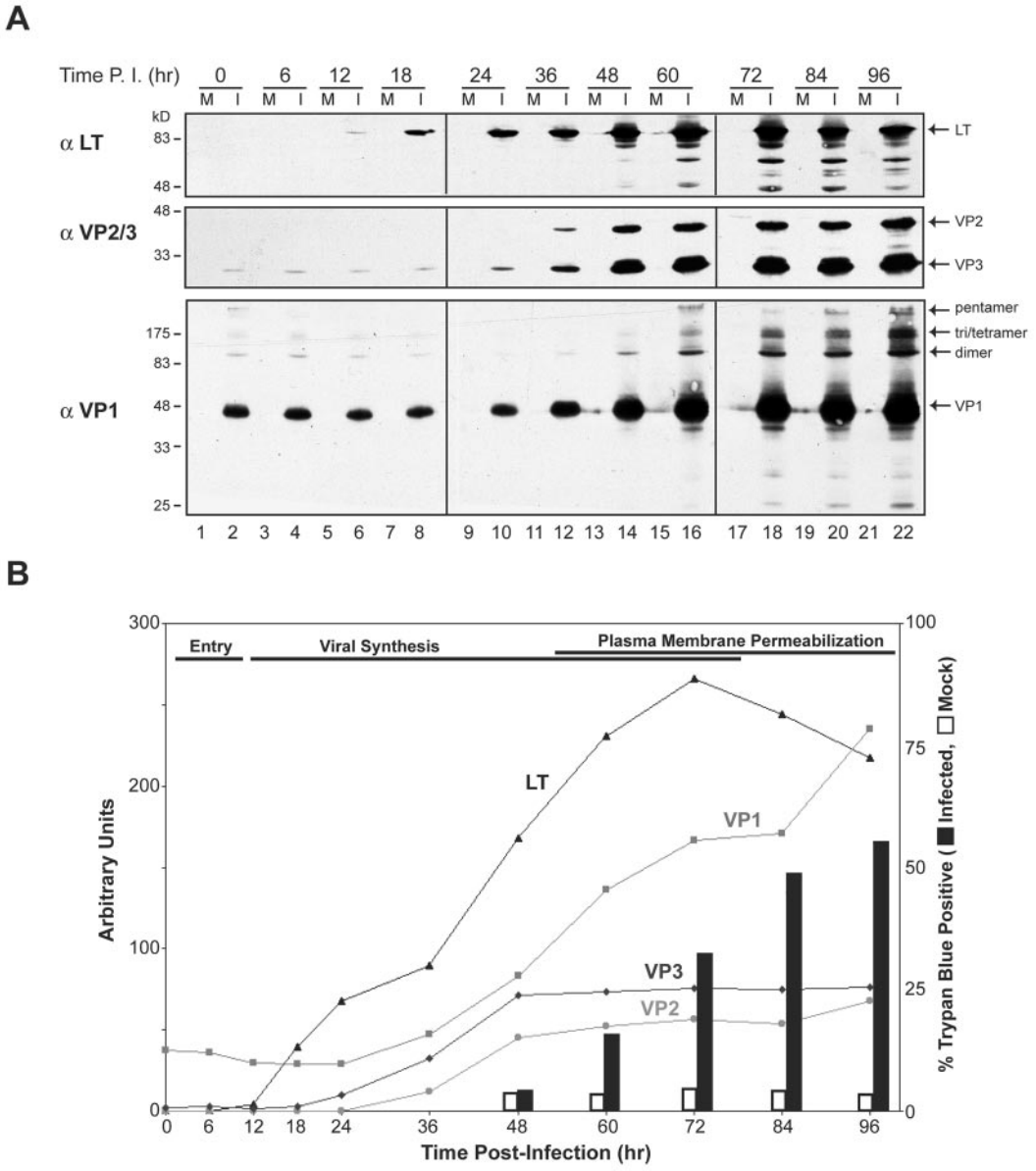

FIG. 1. Temporal analysis of early and late SV40 viral-protein expression and plasma membrane permeabilization after infection. (A) Protein lysates from SV40-infected BS-C-1 cells were immunoblotted with antisera to large T antigen (αLT), VP1 (αVP1), and VP2 and VP3 (αVP2/3). SV40 was bound to confluent monolayers of BS-C-1 cells for 2 h at 4°C, after which the infection medium was removed and replaced with growth medium. Mock (M) and SV40-infected (I) cells were harvested at the indicated times after 4°C binding. Note that VP1 and VP3 were observed from 0 to 24 h postinfection due to their detection from the incoming particles. P.I., postinfection. (B) Quantification of the immunoblots from panel A (lines) and the trypan blue staining of ~1,000 cells that were mock or SV40 infected.

of LT into the medium along with the viral particles. Immunoblotting of the media collected at various times showed significant accumulation of both VP1 and LT starting at 60 h (Fig. 2B, lanes 3 to 6, and Fig. 2C). The presence of VP1 and LT in the media suggested that the residual amounts of VP1 and LT observed at 24 and 48 h were due to the input virus (Fig. 2B, lanes 1 and 2). To confirm that the extracellular presence of VP1 and LT was indicative of infectious SV40 particle release, BS-C-1 cells were infected with 2% of the media samples from 24 to 96 h postinfection and examined for LT production 48 h later. Prior to analysis, the cells were washed and harvested with trypsin to digest residual LT. Infectious SV40 particles were released by 72 h, as LT expression was observed upon infection with the media obtained from 72 to 96 h postinfection (Fig. 2B, lanes 10 to 12). The extracellular appearance of VP1, LT, and infectious SV40 particles, concurrent with the loss of nuclear integrity, implied that SV40 facilitates the release of its progeny by inducing host cell death in a manner that causes nuclear and plasma membrane permeabilization.

SV40 release involves the disruption of the ER membrane. The lipid bilayer surrounding the nucleus is contiguous with

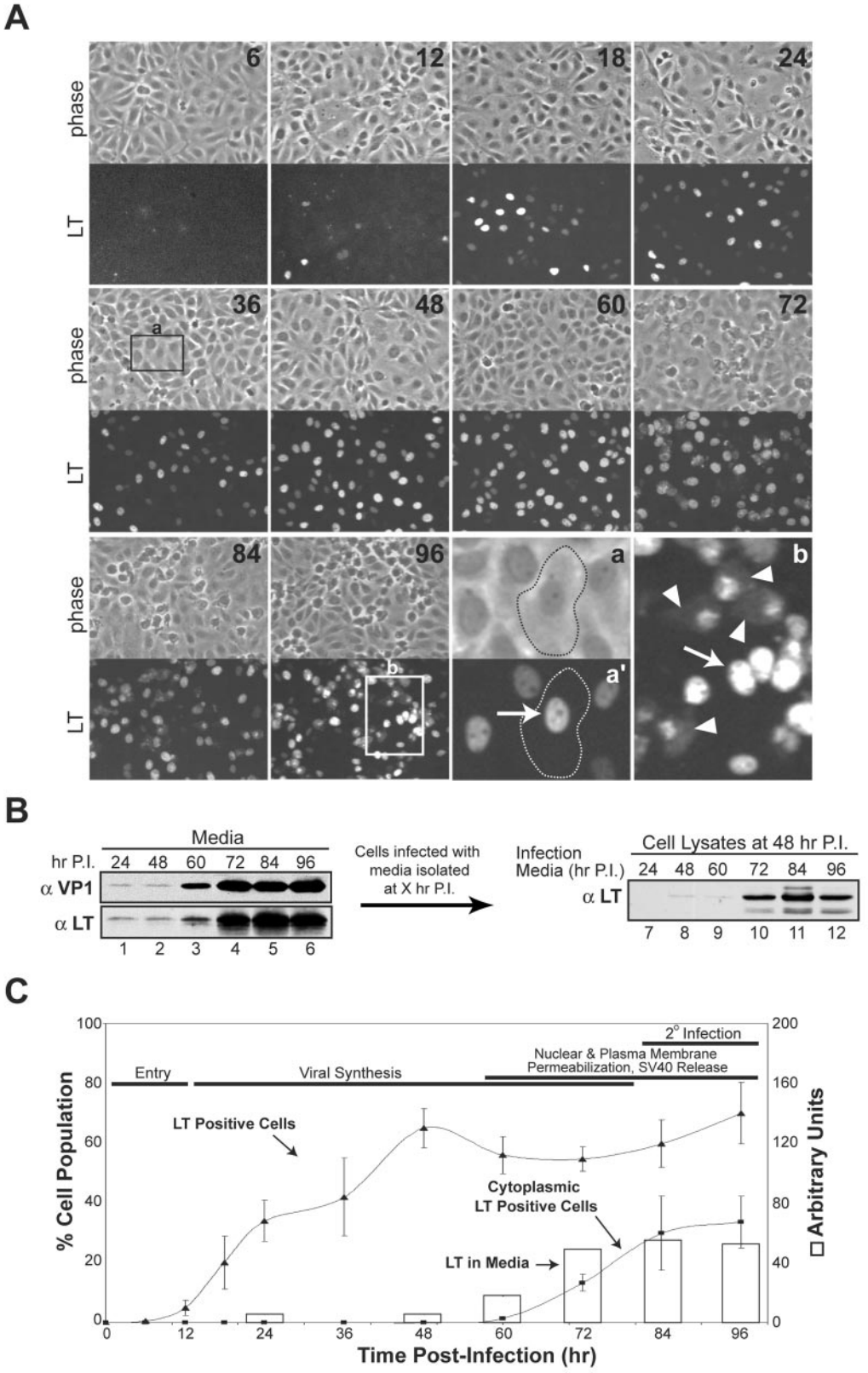

FIG. 2. Large T antigen exits the nucleus and accumulates extracellularly during host cell permeabilization. (A) Confocal microscopy showing the location and population of LT in SV40-infected BS-C-1 cells over time. Coverslips containing confluent BS-C-1 cells were infected as in Fig. 1A, fixed at the indicated time points post-4°C binding with cold 100% MeOH, and immunostained for LT. Representative images showing LT immunofluorescent staining of the corresponding confluent fields (phase contrast) at the indicated times postinfection are displayed. The phase-contrast image in "a" shows the outline of a normal infected cell at 36 h, positive for LT in the nucleus (a', arrow); "b" shows both

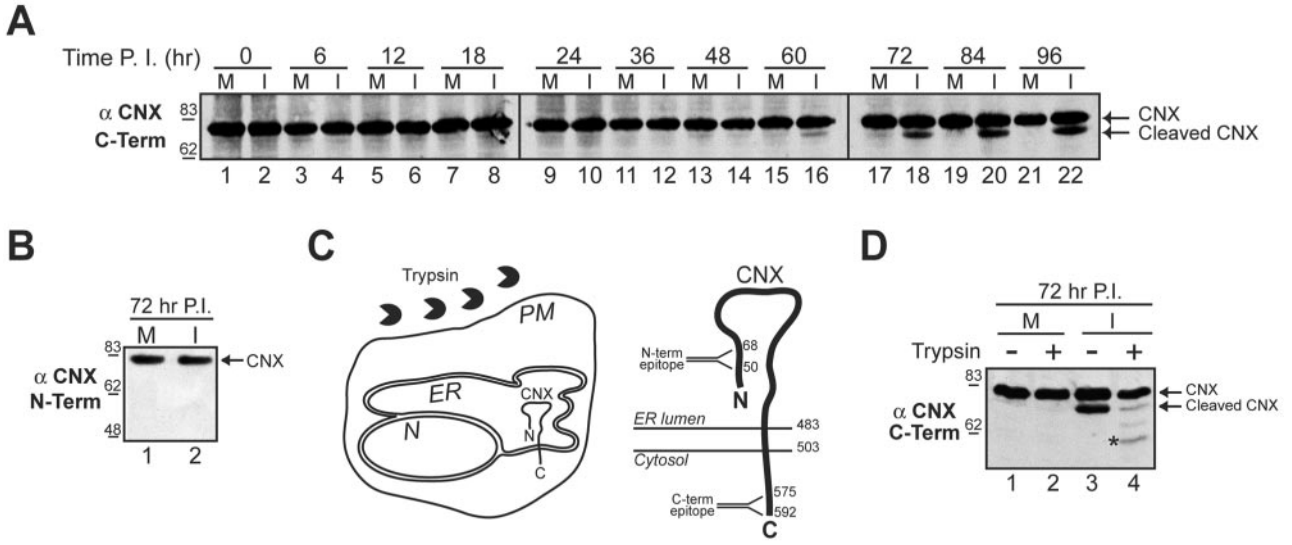

FIG. 3. The ER is ruptured in SV40-infected cells. (A) Cleavage of the ER-resident membrane protein calnexin was monitored by immunoblotting with an antibody to the C terminus of calnexin (αCNX C-term). Confluent BS-C-1 cells were mock (M) or SV40 infected (I) and harvested as in Fig. 1A. (B) Immunoblots of the samples shown in panel A at 72 h postinfection (see lanes 17 and 18) were probed with an antibody to the N terminus of calnexin (αCNX N-term). (C) Diagram of the assay used in panel D showing the addition of trypsin to a cell with respect to the orientation of calnexin within the ER membrane. The larger schematic shows a more detailed topology map of calnexin in the ER membrane, depicting the location of the epitopes for the C- and N-terminal antibodies within the cytosolic and ER-luminal domains, respectively. N, nucleus; PM, plasma membrane; CNX, calnexin. Numbers indicate amino acid residues. (D) Mock (M) or SV40 infected (I) cells at 72 h were treated with trypsin for 15 min where indicated. The cell lysates were separated by SDS-PAGE and probed with the antibody to the C terminus of calnexin. The asterisk indicates a partially trypsinized form of calnexin. Number scale at left in panels A, B, and D indicates molecular mass in kilodaltons. P.I., postinfection.

that of the ER. To determine whether the ER membrane was also disrupted during the permeabilization of the host cell, several ER resident proteins were screened for their stability over the course of infection by immunoblotting (Fig. 3A and data not shown). Antibodies to the cytosolic C terminus of calnexin revealed the presence of a faster-migrating species that began to accumulate at 60 h and was not observed in the mock-infected samples (Fig. 3A, "Cleaved CNX").

The increase in mobility indicated that calnexin was proteolytically cleaved in SV40-infected cells. To determine whether the cleavage occurred within the luminal portion of calnexin, infected-cell lysates at 72 h were probed with antibodies to the N terminus of calnexin (Fig. 3B and C). The N-terminal antibody was unable to recognize the cleaved form of calnexin in the 72-h samples, even though significant amounts were visible using the C-terminal antibody (Fig. 3B, compare lane 2 to Fig. 3A, lane 18). The ability of the C-terminal antibody, but not the N-terminal antibody, to recognize the cleaved form of calnexin indicated that the cleavage of calnexin occurred at its N terminus, which resides within the ER lumen (Fig. 3C).

To test whether the N terminus of calnexin was cleaved in nonviable cells, a trypsin susceptibility assay was performed to examine the integrity of the plasma membrane. In viable cells, calnexin is not accessible to trypsin, but if the plasma and ER membranes have been compromised, then calnexin would be digested by trypsin (Fig. 3C). Mock-infected and infected cells were treated with trypsin at 72 h and the cell lysates were immunoblotted with the C-terminal calnexin antibody. After trypsin treatment, a significant decrease in the abundance of the cleaved form of calnexin was observed (Fig. 3D, compare lane 3 to lane 4). This indicated that the plasma membrane was permeabilized in cells harboring the N-terminal cleaved form of calnexin. The appearance of the faster-migrating partially trypsinized band that retained the C-terminal epitope indicated that the ER membrane was also compromised (Fig. 3D, lane 4, asterisk). Collectively, these data demonstrate that SV40 is released after the induction of host cell death in a manner that causes the permeabilization of the nuclear, ER, and plasma membranes.

permeabilized cells from 96 h with LT in the cytoplasm (arrowheads) and normal nuclear localization (arrow). (B) Immunoblots of the culture media collected at the indicated times postinfection (lanes 1 to 6) and cell lysates harvested at 48 h postinfection with the isolated medium samples (lanes 7 to 12). BS-C-1 cells were infected as in Fig. 1A, the medium was collected at the indicated times, cellular debris was sedimented at 20,000 × *g*, and ~5% of the supernatant was resolved and probed with antisera to LT (αLT) and VP1 (αVP1) (lanes 1 to 6). To test for the presence of infectious particles, BS-C-1 cells were infected with 2% of the supernatant analyzed in lanes 1 to 6, and the cells were washed and harvested by trypsinization at 48 h prior to immunoblotting for the presence of LT (lanes 7 to 12). P.I., postinfection. (C) Quantification of the LT-positive cells and the cells with cytoplasmic LT localization (lines) from panel A and the immunoblots of LT in the culture media from panel B, lanes 1 to 6 (open bars). Fields totaling ~5,000 cells were counted for each time point to calculate the LT-positive percentage shown on the left *y* axis.

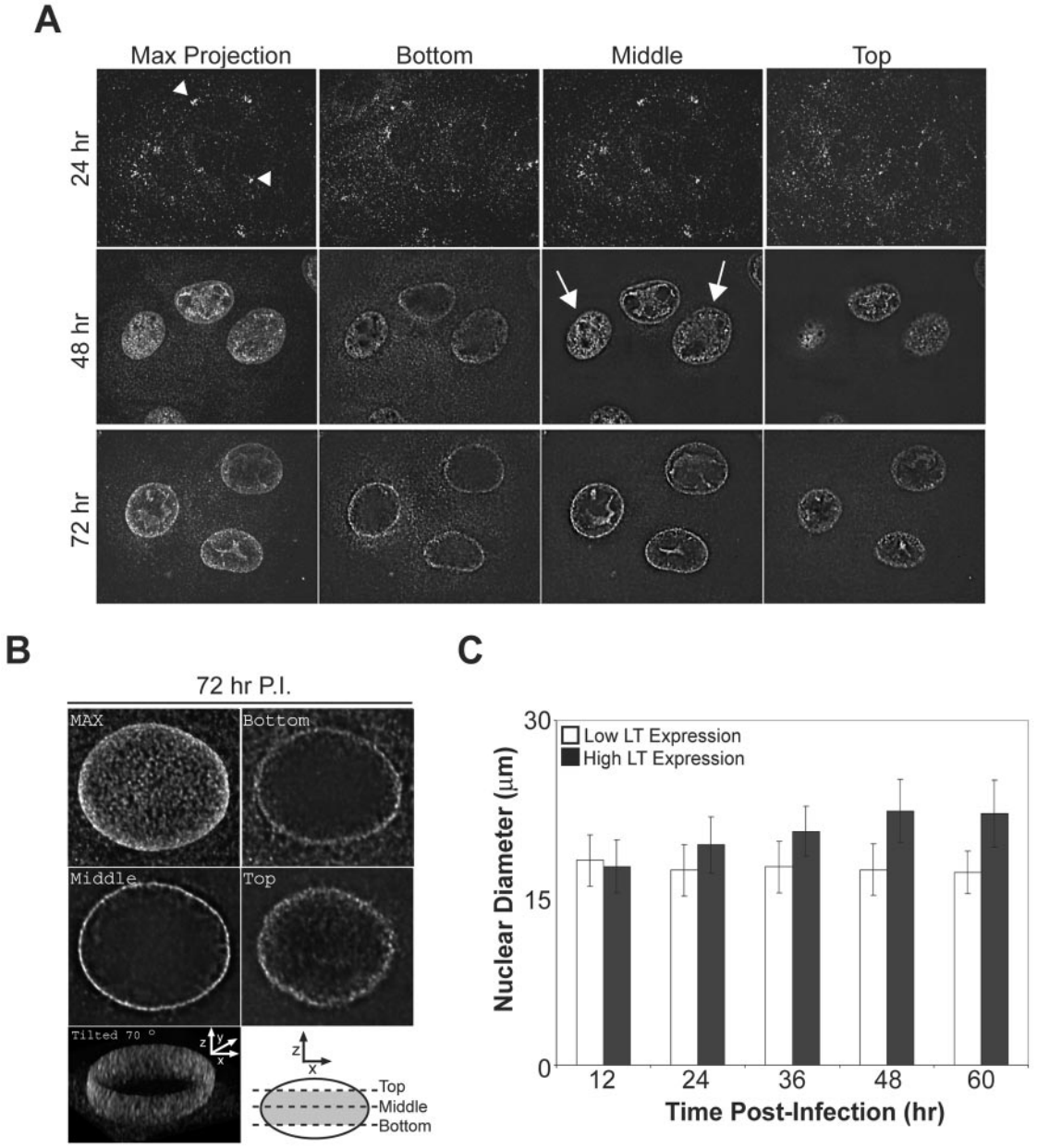

FIG. 4. SV40 egresses to the nuclear envelope after the expansion of the nucleus due to the accumulation of progeny virions. (A) Representative fluorescent images of SV40-infected BS-C-1 cells, fixed at the indicated times postinfection, immunostained for VP1, and examined by confocal microscopy. Serial *z* sections were compiled to produce the "Max Projection" while individual *z* sections from the bottom, middle, and top of the cells are displayed for samples at 48 and 72 h postinfection. The arrowheads indicate the perinuclear accumulation of incoming SV40 and the arrows designate cells with newly synthesized VP1 throughout the nucleus. (B) *z* sections of an infected cell at 72 h postinfection were collected, deconvolved, and reconstructed into a three-dimensional volume. The compilation of the *z* sections is shown in "MAX" and single *z* sections taken according to the diagram from the bottom, middle, and top of the cell are displayed. The two-dimensional projection of the reconstructed three-dimensional volume of the diagrammed section (gray area) was tilted 70° to display the inside of the nucleus. P.I., postinfection. (C) The nuclear diameter of SV40-infected BS-C-1 cells over time with high and low LT expression. Confluent BS-C-1 coverslips were infected as in Fig. 1A, fixed at the indicated time, and immunostained for LT to identify infected cells.

SV40 accumulates at the nuclear envelope prior to cell permeabilization. To examine the cellular localization of SV40 prior to its release, BS-C-1 cells were fixed at various times postinfection, immunostained for the presence of VP1, and analyzed by confocal microscopy. The "Max projection" shows the compilation of the acquired images, while the "Bottom," "Middle," and "Top" were single sections from the respective cell depths indicated by the diagram (Fig. 4B). As a control for incoming virus, cells were first examined at 24 h postinfection (Fig. 4A). During the early stages of late gene expression at 48 h, VP1 was predominantly localized to the nucleus of the infected cell (Fig. 4A, Max Projection). Cross-sectional analy-

sis of these cells revealed that VP1 was excluded from the nucleoli but was present throughout the nucleus in the majority of the cells (Fig. 4A, 48h). As the infection cycle approached completion at 72 h, VP1 staining was no longer evenly distributed throughout the nucleus. Instead, VP1 accumulated around the nuclear envelope (Fig. 4A, 72h). The distribution of VP1 within the nucleus at 72 h postinfection was further investigated by the three-dimensional reconstruction of the nuclear mid-region (Fig. 4B). The three-dimensional image compiled from multiple *z* sections of the nuclear mid-region was tilted 70° to demonstrate the obvious accumulation of VP1 at the nuclear envelope (Fig. 4B). The observed change in the distribution of VP1 from 48 to 72 h suggested that SV40 assembles within the nucleus and then accumulates at the nuclear envelope prior to cell permeabilization. This would advantageously position the particles for release after the permeabilization of the nuclear membrane and death of the host cell.

The size of the nucleus over the course of infection was examined to determine the dynamic swelling of the nucleus with respect to the observed changes in VP1 localization. Cells were immunostained for LT and categorized into two different populations, and their nuclear diameters were measured. High LT expression as measured by fluorescence intensity would correlate to a cell that was later in the infection process, while low LT expression would represent a newly infected cell or a cell that was undergoing a lag in the replication cycle (Fig. 2A, compare 12 to 48 h and 2C). Over the time course examined, the nuclear diameter of cells with low LT expression remained constant at ~17 μm and the diameter of cells with high LT expression increased over time until reaching a plateau at ~22 μm by 48 h (Fig. 4C). These results suggest that the nucleus undergoes an initial expansion during the early stages of viral assembly. The expansion ceased later in the assembly process, when the progeny were found to accumulate at the nuclear envelope prior to cell permeabilization.

SV40 late proteins are required for ER and nuclear membrane permeabilization. The metalloendoprotease inhibitor benzyloxycarbonyl-Gly-Phe-NH_2 (zGF-NH_2) has previously been shown to inhibit SV40 propagation (28). Given that zGF-NH_2 is a protease inhibitor and calnexin was proteolytically cleaved during infection, we analyzed the antiviral properties of this compound in parallel with a variety of other protease inhibitors. Inhibitors that targeted the proteosome (lactacystin, LCT), serine proteases (aprotinin), and aspartic proteases (pepstatin A) were used. SV40-infected BS-C-1 cells were treated with the inhibitors at either 24 or 48 h, and the cells were harvested at 96 h and monitored for calnexin cleavage by immunoblotting.

Strikingly, the SV40-infected cells treated with zGF-NH_2 in 1.4% methanol (MeOH) at 24 or 48 h showed little signs of cytopathology or dead-cell accumulation by 96 h (Fig. 5B, Phase, and data not shown). Calnexin cleavage at 96 h was also prevented by treatment of the infected cells with zGF-NH_2 at these times (Fig. 5A, αCNX C-term, compare lanes 3 and 7 to 1). Upon analysis of viral protein expression, the levels of the early gene LT in the treated samples were roughly equivalent to those in the untreated sample (Fig. 5A, αLT). Similarly, the expression of the late genes (VP1, VP2, and VP3) was comparable in all of the samples with the exception of those treated with zGF-NH_2. Treatment with zGF-NH_2 at 24 h resulted in a marked reduction in viral late gene expression (VP1, VP2, and VP3), while treatment at 48 h showed a moderate decrease at 96 h (Fig. 5A, αVP1 and αVP2/3, compare lanes 3 and 7 to 1).

To investigate whether the nucleus was permeabilized in the samples treated with zGF-NH_2, the localization of LT was examined. Infected BS-C-1 cells treated with zGF-NH_2 at 24 or 48 h and fixed at 96 h showed a morphology that was indistinguishable from that of uninfected cells, while patches of nonviable or dead cells were observed in the MeOH-treated samples (Fig. 5B, Phase, black arrowheads, and data not shown). In the MeOH-treated samples, LT was found to localize within the nucleus of viable infected cells and throughout the cytoplasm in nonviable cells. In contrast, zGF-NH_2-treated cells displayed strict nuclear localization of LT even at 96 h, indicating that the drug inhibited nuclear membrane permeabilization even though the nuclear import of LT was unaffected (Fig. 5B, LT, compare white arrowheads to zGF-NH_2 samples). From these experiments, zGF-NH_2 treatment during SV40 infection was shown to inhibit late gene synthesis and prevent ER and nuclear membrane permeabilization.

zGF-NH_2 inhibits SV40-infected-cell death in a concentration-dependent manner. Next, we asked whether any of the protease inhibitors might prevent the death of SV40-infected cells and release of the virus. The inhibitors were added at 24 or 48 h postinfection. The culture medium from various time points was retained and immunoblotted for VP1 and LT. With the exception of zGF-NH_2-treated samples, VP1 and LT were both present in the medium at concentrations similar to those of the untreated control at 72 h and continued to accumulate by 96 h (Fig. 6A). However, VP1 and LT were both excluded from the culture media when zGF-NH_2 was added at 24 h, while treatment at 48 h showed low extracellular levels of VP1 and LT at 72 h without significant accumulation by 96 h (Fig. 6A, compare lanes 1 through 3 to 7 through 9 and 19 through 21). The exclusion of VP1 from the media after zGF-NH_2 treatment at 24 h could be a direct result of the decreased amount of VP1 within the cells, but LT was also absent and it was found at equivalent levels in the cell (Fig. 5A, αVP1 and αLT, compare lane 1 to lane 3). To test the effects of the various treatments on infectious-particle release, BS-C-1 cells were infected with 2% of the media from the 96-h samples after the various treatments and examined for LT production 48 h postinfection (Fig. 6B and C). As expected, LT production was not observed upon infection with the 96-h media from the cells treated with zGF-NH_2 at 24 h (Fig. 6C, lane 3). However, zGF-NH_2 treatment at 48 h produced infection particles, as LT production was observed in the cells infected with this sample (Fig. 6C, lane 7). These data suggested that zGF-NH_2 treatment at 24 h prevented the permeabilization of SV40-infected cells by inhibiting late gene production.

To directly examine the capacity of zGF-NH_2 to prevent the death of SV40-infected cells, BS-C-1 cells were treated with various concentrations of zGF-NH_2 in MeOH at 24 h and assayed for trypan blue staining at 96 h. Trypan blue staining results of the untreated and MeOH-treated SV40-infected samples were similar, with ~50% of the cells incapable of excluding the dye by 96 h (Fig. 6D). In contrast, zGF-NH_2 treatment resulted in the concentration-dependent inhibition of cell death associated with SV40 infections, as only 7% of the

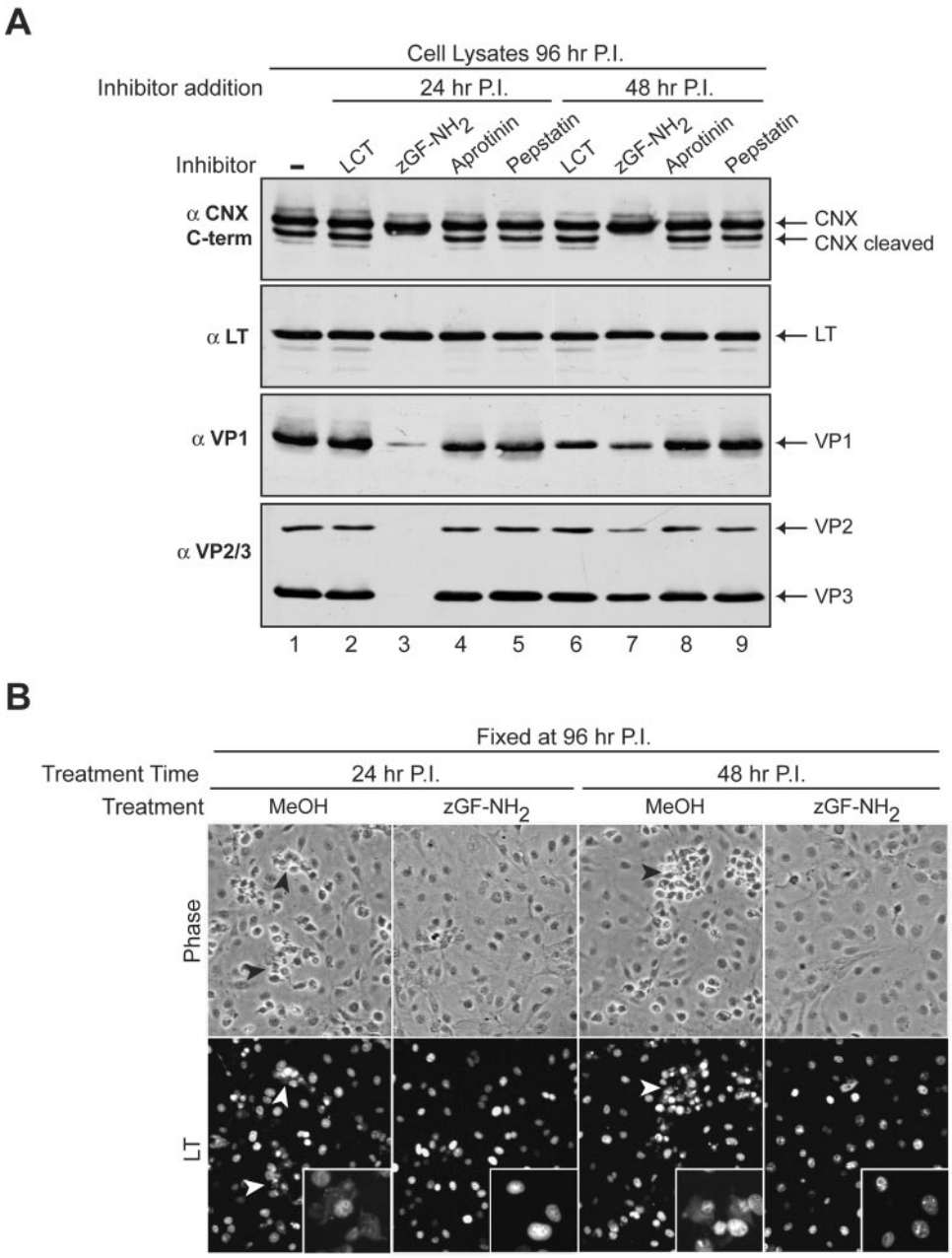

FIG. 5. zGF-NH_2 inhibits SV40 late gene expression, viral-induced calnexin cleavage, and cell death. (A) Immunoblots of cell lysates harvested at 96 h postinfection from confluent BS-C-1 cells either untreated (lane 1) or treated with 1 μM LCT, 2 mM zGF-NH_2 in 1.4% methanol, 5 μM pepstatin A, or 15 μM aprotinin at 24 h (lanes 2 to 5) or 48 h (lanes 6 to 9). The immunoblots were probed with antisera to large T antigen (αLT), VP1 (αVP1), VP2 and VP3 (αVP2/3), and the C terminus of CNX (αCNX). (B) Confluent SV40-infected BS-C-1 coverslips were either mock treated with 1.4% MeOH or treated with 2 mM zGF-NH_2 in 1.4% MeOH at 24 or 48 h postinfection, fixed at 96 h, immunostained for LT, and examined by microscopy. The phase-contrast images are representative fields from the various samples showing the clumps of dead cells (black arrowheads) in samples treated only with MeOH that are absent from those receiving zGF-NH_2 in MeOH. The presence of LT in the corresponding fluorescent images (white arrowheads) shows that these cells are infected. Insets contain higher-magnification images demonstrating the presence of LT outside the nucleus in MeOH-treated samples, while the zGF-NH_2–MeOH-treated samples show strict nuclear LT localization. P.I., postinfection, CNX, calnexin.

cell population was stained by trypan blue when 2 mM zGF-NH_2 was present (Fig. 6D). Supporting this observation, the amount of VP1 and LT present in the culture media by 96 h decreased with the addition of increasing concentrations of zGF-NH_2 added at 24 h (Fig. 6E, compare lanes 3, 5, and 7). Furthermore, the absence of extracellular VP1 and LT at 96 h upon treatment with 2 mM zGF-NH_2 at 24 h correlated with the lack of infectious-particle release, as LT production was not observed in cells infected with this sample (Fig. 6E, compare lane 8 to lane 14). The abilities of zGF-NH_2 treatment to

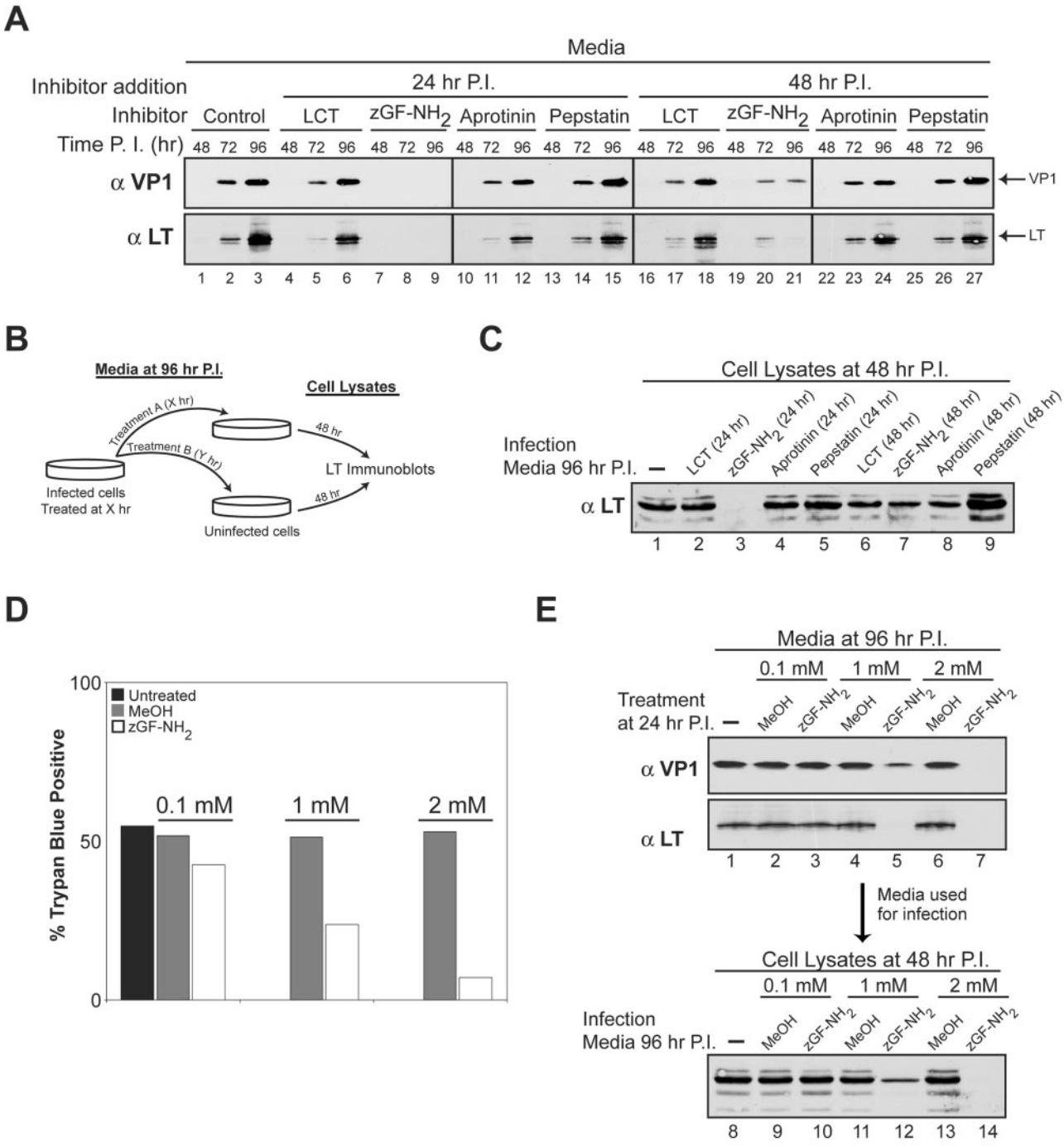

FIG. 6. zGF-NH_2 prevents plasma membrane permeabilization, cell death, and SV40 release. (A) Immunoblots of culture media collected at the indicated time points from BS-C-1 cells infected as in Fig. 1A and either untreated (lane 1 to 3) or treated with 1 μM LCT, 2 mM zGF-NH_2 in MeOH, 5 μM pepstatin A, or 15 μM aprotinin at 24 h (lanes 4 to 15) or 48 h (lanes 16 to 27) postinfection. The media were collected at the indicated times, cellular debris was sedimented at 20,000 × *g*, the supernatant was retained, and ~2% of the total media was resolved and analyzed with antisera to LT (αLT) and VP1 (αVP1). (B) Diagram of the assay used in panel C to test for the presence of infectious-particle release after the various treatments described in the legend to panel A. The media isolated at 96 h from the infected cells after the various treatments were used to infect BS-C-1 cells. Lysates from these cells were harvested at 48 h and analyzed for LT production by immunoblotting. (C) BS-C-1 cells were infected with ~2% of the media isolated at 96 h from previously infected cells that had been subjected to the indicated treatment. At 48 h the cells were washed and trypsinized and the cell lysates were probed with antisera to LT. (D) SV40-infected BS-C-1 cells were either untreated or treated with MeOH or the indicated concentration of zGF-NH_2 in MeOH at 24 h postinfection. Cells were collected at 96 h postinfection and subjected to trypan blue staining. The percentages of ~1,000 cells staining positive for trypan blue are displayed. (E) SV40-infected BS-C-1 cells were either untreated (lane 1) or treated with MeOH (lanes 2, 4, and 6) or the indicated concentration of zGF-NH_2 in MeOH at 24 h postinfection (lanes 3, 5, and 7). The culture media were collected at 96 h postinfection as described in the legend to panel A, immunoblotted for VP1 and LT (lanes 1 to 7), and assayed for the presence of infectious particles (lanes 8 to 14) as described in the legends for panels B and C. P.I., postinfection.

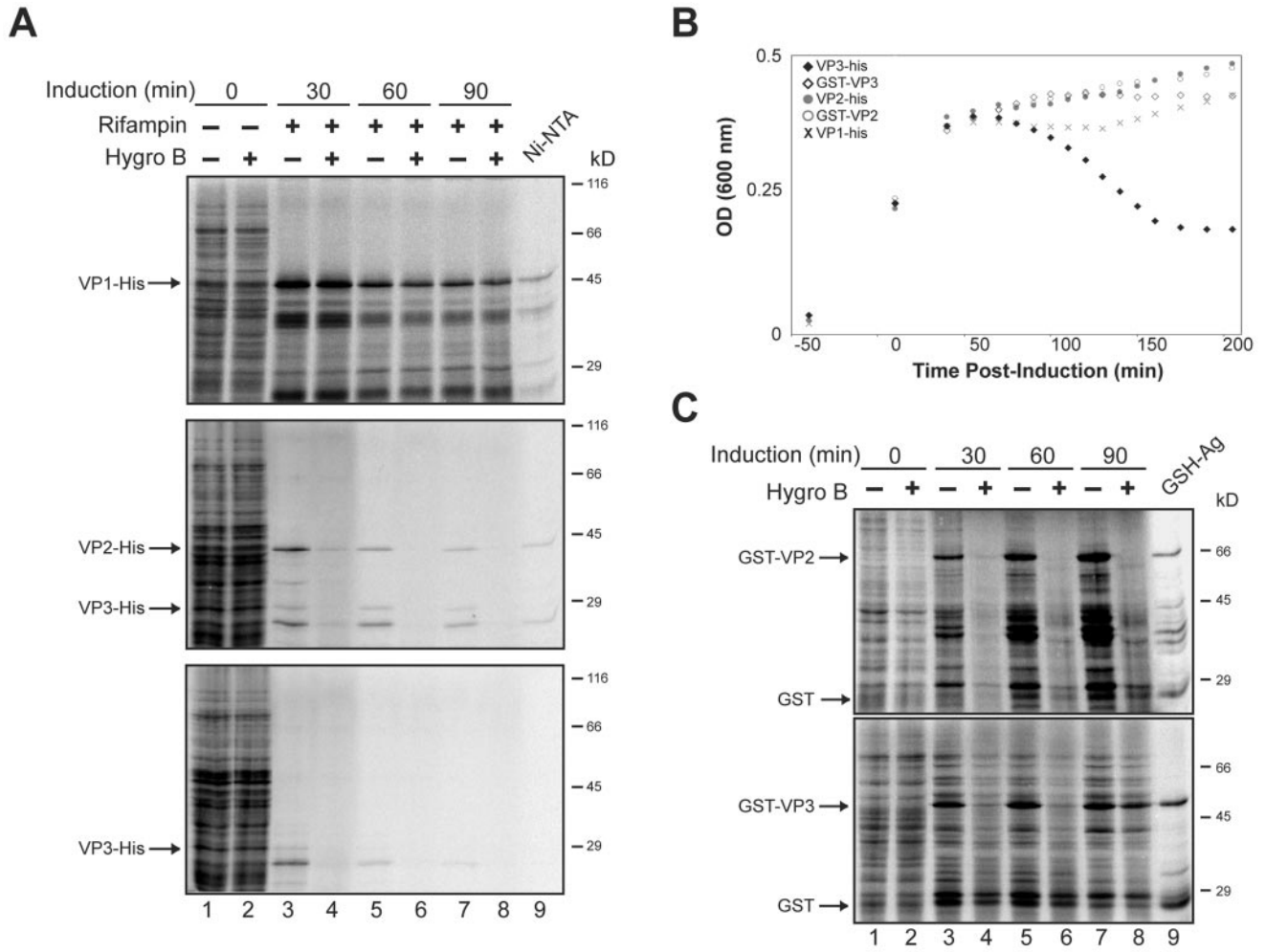

FIG. 7. VP2 permeabilizes *E. coli*, while VP3 permeabilization results in the lysis of the bacterial cells. (A) *E. coli* was pulsed for 10 min with [^{35}S]Met-Cys in the absence or presence of the membrane-impermeable protein synthesis inhibitor hygromycin B prior to inducing the expression of VP1, VP2, or VP3 with C-terminal His tags (lanes 1 and 2) at the indicated time postinduction of these constructs with IPTG (lanes 3 to 8). Rifampin was included during the induction to inhibit endogenous *E. coli* protein synthesis. Bacteria were sedimented, lysed, and resolved by 12% reducing SDS-PAGE followed by autoradiography. Additionally, the expressed protein synthesized 60 min postinduction in the absence of hygromycin B was isolated by Ni-nitrilotriacetic acid Sepharose beads (Ni-NTA). (B) *E. coli* viability was monitored by measuring the OD at 600 nm before and after inducing the expression of VP1, VP2, or VP3 with C-terminal His tags or VP2 and VP3 with N-terminal GST tags. The plots displayed are representative of three independent experiments. (C) *E. coli* containing inducible expression plasmids for GST-VP2 and GST-VP3 was pulsed for 10 min with [^{35}S]Met-Cys in the absence (−) or presence (+) of the membrane-impermeable protein synthesis inhibitor hygromycin B prior to induction, or at the indicated time postinduction with IPTG. Samples were analyzed as in panel A with glutathione-agarose beads used for the isolation. Hygro B, hygromycin B; GSH-Ag, glutathione-agarose.

inhibit synthesis of the late genes (VP1, VP2, and VP3) but not the early gene (LT) and to prevent the permeabilization of SV40 infected cells are supportive of the requirement of the late genes for the death of the host cell.

VP3 expression results in the permeabilization and lysis of bacteria. Expression of the SV40 late proteins appeared to cause the necrotic permeabilization of the host eukaryotic cell. Therefore, we investigated whether the late proteins possessed inherent properties that result in cell permeabilization and death independent of the signaling pathways within the host organism. To address this question, cell permeability of *E. coli* was examined after the individual expression of VP1, VP2, or VP3 containing C-terminal His tags driven by a T7 promoter. The integrity of the *E. coli* double-membrane barrier was analyzed by determining the sensitivity of protein synthesis to the membrane-impermeable protein synthesis inhibitor hygromycin B (8).

Prior to induction, the *E. coli* cells were pulsed with [^{35}S]Met-Cys for 10 min in the absence or presence of hygromycin B, and no change in protein synthesis was observed (Fig. 7A, compare lanes 1 and 2). To ensure that these results directly correlated to the expression of VP1, VP2, or VP3, rifampin was also added during the induction to inhibit the *E. coli* RNA polymerase and prevent the synthesis of endogenous bacterial proteins. Since rifampin takes ~20 min to completely inhibit the *E. coli* RNA polymerase, we found that the T7 produced within this time period was sufficient for expression of the tagged constructs over the examined time period (data not shown). Isolation of the expressed protein provided evi-

dence that the His-tagged VP1 and VP2 were present 60 min after induction (Fig. 7A, lane 9). Over time, the expression of VP1 had no effect on the permeability of the *E. coli* bacteria, as protein synthesis was not inhibited by the addition of hygromycin B. In contrast, VP2 and VP3 expression resulted in the permeabilization of *E. coli* as protein synthesis was inhibited in the presence of hygromycin B (Fig. 7A, lanes 3 to 8). Therefore, VP2 and VP3 caused the permeabilization of *E. coli* membranes.

The permeabilization of cellular membranes can lead to cell lysis or death. Therefore, we investigated the viability of the *E. coli* after the induction of VP1, VP2, or VP3 expression to determine whether these late viral proteins possess lytic properties. Strikingly, ~60 min after the induction of VP3 expression, a time-dependent increase in bacterial cell lysis was observed by monitoring the OD at 600 nm (Fig. 7B, filled diamonds). This explained the decrease in VP3 synthesis observed over time even in the absence of hygromycin B (Fig. 7A). In contrast, the induction of VP1 or VP2 expression did not cause lysis of the bacteria, as no decrease in the OD was observed. Instead, the OD reached a plateau at 45 min indicative of bacterial stasis, as replication ceased due to the utilization of the cellular machinery for protein expression (Fig. 7B).

It is not surprising that VP2 and VP3 possess similar properties, since VP2 is essentially VP3 with a ~120-amino-acid extension to its N terminus. Interestingly, while VP2 and VP3 were both capable of permeabilizing *E. coli*, the extra ~120 amino acids on the N terminus of VP2 apparently inhibited its lytic properties. In support of this point, VP3 with an N-terminal glutathione *S*-transferase (GST) tag (~220 amino acids) was also incapable of inducing bacterial lysis (Fig. 7B, open diamonds). Analysis of *E. coli* permeabilization upon the induction of GST-VP3 expression revealed that GST-VP3 behaved similarly to VP2. It rendered the bacteria permeable to hygromycin B but did not support cell lysis (Fig. 7C and B). An intriguing observation was that the permeabilization properties of GST-VP3 decreased with increasing amounts of GST-VP3 (Fig. 7C, compare lanes 4, 6, and 8). Therefore, the N terminus of VP2 inhibited the lytic properties of VP3. Together, these data indicated that VP2 and VP3 were capable of permeabilizing bacteria and that VP3 possesses an inherent lytic property.

DISCUSSION

The major findings of this study are that permeabilization of the nuclear, ER, and plasma membranes that is characteristic of necrosis correlated temporally with the appearance of the SV40 late gene products and was not observed upon their selective inhibition. These experimental observations raise the possibility that one or more of the late gene products has the inherent ability to induce the observed changes in the host membrane permeability. That premise was tested by separately expressing the late gene products VP1, VP2, and VP3 in *E. coli*. These results demonstrated that VP2 and VP3, but not VP1, possessed membrane-permeabilizing activity in prokaryotic cells. Furthermore, the ability to induce bacterial lysis following permeabilization was an exclusive property of VP3. We conclude that membrane permeability changes induced by VP3, and perhaps VP2 as well, are largely responsible for the necrosis resulting from SV40 infection and that the lytic activity of VP3 may be necessary for the release of progeny virions.

The temporal analysis of the SV40 life cycle revealed that the viral replication process directed the death of the infected cells in a scheduled manner. At any given time during the initiation of viral gene expression (0 to 48 h), the percentage of the population expressing LT directly correlated to the percentage of dead cells observed 48 h later (Fig. 1B and 2C). Therefore, the variation in the timing of LT expression appeared to be responsible for the broad time range for viral-induced cell death (60 to 96 h). In addition, treatment with the metalloendoprotease inhibitor zGF-NH_2 prevented synthesis of the late genes but not the early genes. The inhibition of protein synthesis by zGF-NH_2 has previously been observed for other proteins (4, 14, 17). In our study, zGF-NH_2 inhibition of late gene synthesis prevented the permeabilization and death of SV40-infected cells, supporting the requirement of late protein synthesis for cell death.

The observations that cell death required late protein synthesis and that it occurred at a specified time during viral replication suggested that cell death was likely dependent on the concentration of the late proteins. This was further supported by inhibiting the accumulation of the late gene products just prior to cell death at 60 h, by treating the cells with zGF-NH_2 at 48 h. Here, we observed only a small degree of membrane permeabilization as low levels of VP1 and LT were present extracellularly at 72 h without accumulation from 72 to 96 h (Fig. 6A, lanes 20 and 21). Due to the fact that infectious particles were released (Fig. 6C, lane 7) and some cell death still occurred after treatment with zGF-NH_2 at 48 h, which is 12 h prior to cell death, it is unlikely that this drug inhibits a signaling pathway required for cell death. More likely, there is a strict requirement for a given concentration of late proteins to induce cell death, and the addition of zGF-NH_2 at 24 h inhibited the cell from reaching that critical threshold.

There are two pathways for cell death in eukaryotic cells (reviewed in references 23 and 25). Apoptotic cell death results in DNA fragmentation and the concealment of the cellular constituents in membrane-enclosed spherical bodies. Alternatively, necrotic cell death is characterized by cellular swelling, fragmentation of the rough ER, and permeabilization of the plasma membrane resulting in the release of cytosolic constituents into the extracellular environment (33, 34). Given these criteria, necrosis would appear to be a more beneficial pathway for nonenveloped viral release. Apoptosis would cause the exposed viral genomes to be degraded and the viral progeny to be encapsulated by cellular membranes, inhibiting their ability to initiate secondary infections. However, necrosis would result in the breaching of the cellular membrane barriers surrounding the progeny, facilitating their release in an infectious state.

Several of our findings are consistent with the host initiating a necrotic response to late gene expression. Swelling of the nucleus was observed after late gene synthesis and prior to cell death. Permeability changes in the plasma, nuclear, and ER membranes occurred after late gene synthesis and were absent upon the selective inhibition of these viral gene products. While these results can be explained by necrosis, they do not indicate that SV40 activated a cellular pathway that resulted in necrosis.

In uninfected cells, the overstimulation of poly(ADP-ribose) polymerase-1 (PARP) due to DNA strand breaks leads to an irreversible NAD^+ depletion that results in cellular necrosis (2, 5). A previous study indicated that VP3 might induce necrosis by stimulating PARP (12). Specifically, GST-VP3 bound and stimulated the in vitro autoribosylation activity of PARP. In addition, PARP inhibition during SV40 infections resulted in a slight decrease in the production of extracellular infectious particles and cytopathic effects. Our findings do not dispute this earlier report. However, they show that the lytic activity of VP3 and possibly VP2 is an inherent property of the proteins themselves irrespective of any eukaryotic signaling or cell death program. This was demonstrated by the fact that these proteins displayed lytic activity in *E. coli*, where PARP or related pathways are absent (5, 18). Therefore, these proteins might be involved in facilitating the release of the progeny.

In this study, we used LT as a nuclear-protein marker and found that it accumulated extracellularly in concert with the viral late proteins starting at 60 h. Analysis of ER-resident proteins revealed that BiP (the ER hsp70 family member) and calreticulin also accumulated extracellularly (data not shown) and that the ER-luminal domain of calnexin was cleaved in a time-dependent manner starting at 60 h. Since the ER lacks promiscuous proteases, calnexin cleavage appeared to be a signature of ER permeabilization. This was also supported by the accessibility of the ER-luminal domain of calnexin to extracellular trypsin (Fig. 3D, lane 4). Together, these results indicate that the SV40 life cycle leads to the permeabilization of the ER, nuclear, and plasma membranes, accounting for the ability of the progeny to pass from the nucleus to the extracellular environment.

Viral propagation is dictated by the number of infectious particles that are released in a given time period. The duration of the life cycle has a stronger influence on viral propagation than the number of particles released over time, as has been well established for bacteriophage replication and release (35). Thus, the most efficient propagation involves short-life cycle time spans that create an exponential rise in progeny production. Here, we demonstrate that the release of the nonenveloped SV40 progeny is regulated by the lytic properties of the late proteins. This enables the strict parameters for viral gene expression to dictate the occurrence of host cell lysis and viral release to a time that promotes the most efficient propagation. In support of this hypothesis, stable cell lines expressing the nonstructural proteins (LT, ST, and the agnoprotein) have been established, arguing against their ability to induce cell death (6, 7, 22, 24, 31). Further studies will be needed to explore how the late viral proteins direct the timely execution of cell permeabilization and death.

ACKNOWLEDGMENTS

We thank members of the Hebert lab and Kristen Vella for critical reading of the manuscript.

This work was supported in part by US Public Health grant CA79864 and a University of Massachusetts Faculty Research Grant (to D.N.H.). R.D. was partially supported by an NIH Chemistry-Biology Interface training grant (T32GM00815). In addition, P.W. and L.C.N. were supported by US Public Health grants GM59057 and CA100479, respectively.

REFERENCES

1. **Barouch, D. H., and S. C. Harrison.** 1994. Interactions among the major and minor coat proteins of polyomavirus. J. Virol. **68:**3982–3989.
2. **Berger, N. A.** 1985. Poly(ADP-ribose) in the cellular response to DNA damage. Radiat. Res. **101:**4–15.
3. **Brady, J., J. B. Bolen, M. Radonovich, N. Salzman, and G. Khoury.** 1984. Stimulation of simian virus 40 late gene expression by simian virus 40 tumor antigen. Proc. Natl. Acad. Sci. USA **81:**2040–2044.
4. **Brostrom, M. A., C. R. Prostko, D. Gmitter-Yellen, L. J. Grandison, G. Kuznetsov, W. L. Wong, and C. O. Brostrom.** 1991. Inhibition of translational initiation by metalloendoprotease antagonists. Evidence for involvement of sequestered Ca2+ stores. J. Biol. Chem. **266:**7037–7043.
5. **Burkle, A.** 2005. Poly(ADP-ribose). The most elaborate metabolite of NAD+. FEBS J. **272:**4576–4589.
6. **Butel, J. S., and J. A. Lednicky.** 1999. Cell and molecular biology of simian virus 40: implications for human infections and disease. J. Natl. Cancer Inst. **91:**119–134.
7. **Carswell, S., J. Resnick, and J. C. Alwine.** 1986. Construction and characterization of CV-1P cell lines which constitutively express the simian virus 40 agnoprotein: alteration of plaquing phenotype of viral agnogene mutants. J. Virol. **60:**415–422.
8. **Chang, Y.-S., C.-L. Liao, C.-H. Tsao, M.-C. Chen, C.-I. Liu, L.-K. Chen, and Y.-L. Lin.** 1999. Membrane permeabilization by small hydrophobic nonstructural proteins of Japanese encephalitis virus. J. Virol. **73:**6257–6264.
9. **Chen, X. S., T. Stehle, and S. C. Harrison.** 1998. Interaction of polyomavirus internal protein VP2 with the major capsid protein VP1 and implications for participation of VP2 in viral entry. EMBO J. **17:**3233–3240.
10. **Eggleton, K. H., and L. C. Norkin.** 1981. Cell killing by simian virus 40: the sequence of ultrastructural alterations leading to cellular degeneration and death. Virology **110:**73–86.
11. **Fiers, W., R. Contreras, G. Haegemann, R. Rogiers, A. Van de Voorde, H. Van Heuverswyn, J. Van Herreweghe, G. Volckaert, and M. Ysebaert.** 1978. Complete nucleotide sequence of SV40 DNA. Nature **273:**113–120.
12. **Gordon-Shaag, A., Y. Yosef, M. Abd El-Latif, and A. Oppenheim.** 2003. The abundant nuclear enzyme PARP participates in the life cycle of simian virus 40 and is stimulated by minor capsid protein VP3. J. Virol. **77:**4273–4282.
13. **Granboulan, N., P. Tournier, R. Wicker, and W. Bernhard.** 1963. An electron microscope study of the development of SV40 virus. J. Cell Biol. **17:**423–441.
14. **Ivessa, N. E., C. De Lemos-Chiarandini, D. Gravotta, D. D. Sabatini, and G. Kreibich.** 1995. The brefeldin A-induced retrograde transport from the Golgi apparatus to the endoplasmic reticulum depends on calcium sequestered to intracellular stores. J. Biol. Chem. **270:**25960–25967.
15. **Kasamatsu, H., and A. Nakanishi.** 1998. How do animal DNA viruses get to the nucleus? Annu. Rev. Microbiol. **52:**627–686.
16. **Keller, J. M., and J. C. Alwine.** 1984. Activation of the SV40 late promoter: direct effects of T antigen in the absence of viral DNA replication. Cell **36:**381–389.
17. **Kuznetsov, G., M. Brostrom, and C. O. Brostrom.** 1992. Demonstration of a calcium requirement for secretory protein processing and export. Differential effects of calcium and dithiothreitol. J. Biol. Chem. **267:**3932–3939.
18. **Lewis, K.** 2000. Programmed death in bacteria. Microbiol. Mol. Biol. Rev. **64:**503–514.
19. **Liddington, R. C., Y. Yan, J. Moulai, R. Sahli, T. L. Benjamin, and S. C. Harrison.** 1991. Structure of simian virus 40 at 3.8-Å resolution. Nature **354:**278–284.
20. **Lin, W., T. Hata, and H. Kasamatsu.** 1984. Subcellular distribution of viral structural proteins during simian virus 40 infection. J. Virol. **50:**363–371.
21. **Matthopoulos, D. P., and G. N. Pagoulatos.** 1988. Variable expression of SV40 large T antigen in CV1 cell clones. FEBS Lett. **232:**177–181.
22. **Obinata, M.** 1997. Conditionally immortalized cell lines with differentiated functions established from temperature-sensitive T-antigen transgenic mice. Genes Cells **2:**235–244.
23. **Padanilam, B. J.** 2003. Cell death induced by acute renal injury: a perspective on the contributions of apoptosis and necrosis. Am. J. Physiol. Renal Physiol. **284:**F608–F627.
24. **Phillips, B., and K. Rundell.** 1988. Failure of simian virus 40 small t antigen to disorganize actin cables in nonpermissive cell lines. J. Virol. **62:**768–775.
25. **Proskuryakov, S. Y., A. G. Konoplyannikov, and V. L. Gabai.** 2003. Necrosis: a specific form of programmed cell death? Exp. Cell Res. **283:**1–16.
26. **Reddy, V. B., B. Thimmappaya, R. Dhar, K. N. Subramanian, B. S. Zain, J. Pan, P. K. Ghosh, M. L. Celma, and S. M. Weissman.** 1978. The genome of simian virus 40. Science **200:**494–502.
27. **Resnick, J., and T. Shenk.** 1986. Simian virus 40 agnoprotein facilitates normal nuclear location of the major capsid polypeptide and cell-to-cell spread of virus. J. Virol. **60:**1098–1106.
28. **Richards, A. A., E. Stang, R. Pepperkok, and R. G. Parton.** 2002. Inhibitors of COP-mediated transport and cholera toxin action inhibit simian virus 40 infection. Mol. Biol. Cell **13:**1750–1764.
29. **Rosenthal, L. J., and M. Brown.** 1977. The control of SV40 transcription

during a lytic infection: late RNA synthesis in the presence of inhibitors of DNA replication. Nucleic Acids Res. **4:**551–565.
30. **Smith, A. E., and A. Helenius.** 2004. How viruses enter animal cells. Science **304:**237–242.
31. **Takeuchi, K., K. Sakurada, H. Endou, M. Obinata, and M. P. Quinlan.** 2002. Differential effects of DNA tumor virus genes on the expression profiles, differentiation, and morphogenetic reprogramming potential of epithelial cells. Virology **300:**8–19.
32. **Tegtmeyer, P.** 1972. Simian virus 40 deoxyribonucleic acid synthesis: the viral replicon. J. Virol. **10:**591–598.
33. **Trump, B. F., P. J. Goldblatt, and R. E. Stowell.** 1965. Studies of mouse liver necrosis in vitro. Ultrastructural and cytochemical alterations in hepatic parenchymal cell nuclei. Lab. Investig. **14:**1969–1999.
34. **Trump, B. F., P. J. Goldblatt, and R. E. Stowell.** 1965. Studies of necrosis in vitro of mouse hepatic parenchymal cells. Ultrastructural alterations in endoplasmic reticulum, Golgi apparatus, plasma membrane, and lipid droplets. Lab. Investig. **14:**2000–2028.
35. **Wang, I. N., D. L. Smith, and R. Young.** 2000. Holins: the protein clocks of bacteriophage infections. Annu. Rev. Microbiol. **54:**799–825.
36. **Whittaker, G. R., M. Kann, and A. Helenius.** 2000. Viral entry into the nucleus. Annu. Rev. Cell Dev. Biol. **16:**627–651.
37. **Xu, M., D. K. Struck, J. Deaton, I. N. Wang, and R. Young.** 2004. A signal-arrest-release sequence mediates export and control of the phage P1 endolysin. Proc. Natl. Acad. Sci. USA **101:**6415–6420.
38. **Yu, Y., S. B. Kudchodkar, and J. C. Alwine.** 2005. Effects of simian virus 40 large and small tumor antigens on mammalian target of rapamycin signaling: small tumor antigen mediates hypophosphorylation of eIF4E-binding protein 1 late in infection. J. Virol. **79:**6882–6889.